Physics of Fluids

RESEARCH ARTICLE | MARCH 07 2023

On the cylinder noise and drag reductions in different Reynolds number ranges using surface pattern fabrics

Chuntai Zheng (郑春泰) ; Peng Zhou (周朋) ; Siyang Zhong (钟思阳) ; Xin Zhang (张欣)

Check for updates

Physics of Fluids 35, 035111 (2023)
https://doi.org/10.1063/5.0138074

View Online
Export Citation

Articles You May Be Interested In

Experimental investigation on cylinder noise and its reductions by identifying aerodynamic sound sources in flow fields

Physics of Fluids (March 2023)

An experimental investigation of drag and noise reduction from a circular cylinder using longitudinal grooves

Physics of Fluids (November 2021)

Intrinsic features of flow around two side-by-side square cylinders

Physics of Fluids (August 2013)

13 January 2025 06:10:20

AIP Publishing

AIP Publishing
Physics of Fluids
Special Topics Open for Submissions
Learn More

Physics of Fluids ARTICLE scitation.org/journal/phf

On the cylinder noise and drag reductions in different Reynolds number ranges using surface pattern fabrics

Cite as: Phys. Fluids **35**, 035111 (2023); doi: 10.1063/5.0138074
Submitted: 8 December 2022 · Accepted: 13 February 2023 ·
Published Online: 7 March 2023

View Online Export Citation CrossMark

Chuntai Zheng (郑春泰),[1] Peng Zhou (周朋),[1] Siyang Zhong (钟思阳),[2] and Xin Zhang (张欣)[1,a)]

AFFILIATIONS

[1]Department of Mechanical and Aerospace Engineering, The Hong Kong University of Science and Technology, Clear Water Bay, Kowloon, Hong Kong, China
[2]Department of Aeronautical and Aviation Engineering, The Hong Kong Polytechnic University, Hung Hom, Kowloon, Hong Kong, China

[a)]Author to whom correspondence should be addressed: aexzhang@ust.hk

ABSTRACT

This study experimentally investigates the potential of using surface pattern fabrics for the cylinder noise and drag control in different Reynolds number ranges. The aerodynamic and aeroacoustic effects were evaluated through the noise and force measurements in an anechoic wind tunnel. It was observed that the noise and drag reductions take place simultaneously but in different Reynolds number ranges, corresponding to the cylinder flow in different flow regimes, e.g., sub-critical, critical, and supercritical flow regimes. Microphone arc array measurements reveal that the suppression of the Aeolian tone in the critical regime is the major cause of noise reductions, and the noise directivity gradually loses dipole features in the critical and supercritical flow regimes, which is probably related to the reduced lift fluctuation coefficient and the spanwise segment of the sound sources. Further hotwire wake survey revealed significant changes in flow dynamics, which explain the variations of noise and drag in different flow regimes. We have shown for the first time that fabric with different surface patterns can effectively reduce cylinder drag and noise in different Reynolds number ranges. Since the Reynolds number is a key factor that determines the flow state in practical engineering applications, e.g., cycling aerodynamics, this study suggests that optimal drag and noise reductions can be realized by employing the combinations of different surface pattern fabrics to account for the Reynolds number effects.

Published under an exclusive license by AIP Publishing. https://doi.org/10.1063/5.0138074

13 January 2025 06:10:20

I. INTRODUCTION

Noise and drag reductions of flow over a bluff body are important in many applications,[1] such as drag reduction from a cyclist,[2] noise reduction from a pantograph of a train,[3] and noise reduction from a side-view mirror.[4] A circular cylinder is a representative shape of bluff bodies, and many efforts have been made to control a cylinder flow to achieve drag and noise reductions.[1,5,6] The cylinder flow is chosen for the study as it presents a generic bluff-body flow feature, and principles and control methods can be used for practical engineering applications.

Various passive control methods were proposed for controlling drag and noise on a circular cylinder. Research shows that increasing surface roughness[7–9] and adding surface patterns, such as grooves,[10,11] dimples,[12,13] and helical wire,[14] are able to reduce drag on a circular cylinder by forcing flow transition in a certain Reynolds number range, resulting in delayed flow separations.[5]

Based on flow transition processes, a cylinder flow can be classified into different flow regimes,[5,15] e.g., sub-critical, critical, and supercritical regimes. As shown in Fig. 1, the sub-critical flow regime is featured by the almost constant drag coefficient (C_D). In this regime, the boundary layer remains laminar until separation and the transition to turbulence happens in the separated shear layers. When increasing the Reynolds number, the transition to turbulence gradually happens before the separation, which delays the flow separation. It further leads to the occurrence of the drag crisis (C_D has sudden drops), which denotes the cylinder flow in the critical regime. Bearman[16] shows two major drops of C_D in the critical regime. The first drop is accompanied by an asymmetric flow state where a laminar separation bubble forms on one side of the cylinder only.[16,17] The second drop is associated with the formation of separation bubbles on both sides, by which the flow recovers symmetry.[16,17] Followed by the critical regime, the supercritical regime is characterized by the increase in C_D and the fully

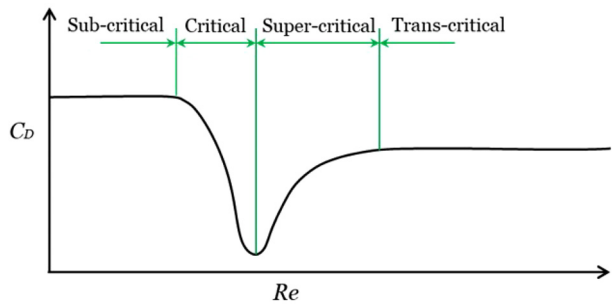

FIG. 1. Definition of flow regimes for the flow past circular cylinder.

turbulent boundary layer before the separation, by which the flow is symmetric and the regular vortex shedding may reoccur.[16,18,19]

Usually, the flow transition either in the shear layers or boundary layers can significantly change the unsteady flow dynamics, e.g., vortex shedding, by which the noise radiation properties of a circular cylinder can also be affected. By these principles, various passive control methods, including porous materials,[20–23] a splitter plate,[24–26] wavy structures,[27] and helical cables,[28] are widely used to reduce the cylinder noise. Particularly, recent research first reveals that small surface patterns, i.e., longitudinal grooves built on a piece of fabric, can be used to simultaneously reduce cylinder noise and drag in a certain Reynolds number range,[6] and it can be potentially used for a low-drag skin suit design in cycling. However, its control effects are highly dependent on Reynolds numbers. For example, it has little effect on cylinder drag and noise reductions in the sub-critical flow regime, while it achieves the maximum drag and noise reductions at the end of the critical regime. The Reynolds number is a key factor determining the flow states over a bluff body,[5,29,30] by which the effectiveness of flow control methods is changed in different Reynolds number ranges. For example, since the Reynolds number of a cyclist (bluff body) is influenced by cycling speeds and sizes of limbs,[31] the fabric selection for designing a low-drag skin suit design requires the knowledge of the aerodynamic properties of fabrics at different Reynolds numbers. Moreover, an aircraft landing gear noise contains noise contributions from different components, such as struts, the wheels, and wires, and flow over these components has different Reynolds numbers based on their geometric dimensions.[32] The capabilities of controlling noise and drag in a selected Reynolds number range are essential for optimized flow control in engineering applications.

There are still several unresolved questions on this research topic that need further investigation. The first question is whether we can use fabrics with different surface patterns to simultaneously control the drag and noise reductions on a circular cylinder in different Reynolds number ranges. The second is how surface pattern fabrics influence the cylinder noise directivity corresponding to the flow in different flow regimes. Answering these questions helps to enhance the understanding of drag and noise reductions on a circular cylinder using surface pattern fabrics. It is also beneficial for achieving maximum noise and drag reductions in engineering applications, e.g., customizing a skin suit made from different types of surface pattern fabrics according to the Reynolds number of a cyclist.

In this study, six fabrics with different surface patterns (surface pattern fabric) are attached to a circular cylinder to reduce cylinder noise and drag, and their control effects are investigated through anechoic wind tunnel tests at different Reynolds numbers. Their influences on noise directivity in different flow regimes are investigated by the microphone arc array measurement. In the rest of the paper, Sec. II introduces the setup of wind tunnel tests; Sec. III shows the force, noise, and wake measurement results for the cylinder with different surface pattern fabrics, based on which discussions are made; Sec. IV provides the conclusions.

II. EXPERIMENT SETUP

A. Anechoic wind tunnel and test model

Measurements were conducted in an anechoic wind tunnel (UNITED),[33,34] at the Hong Kong University of Science and Technology (HKUST). An open-jet test section with a square outlet of $0.4 \times 0.4\,m^2$ was used for the experiment. The turbulence intensity is lower than 0.25%. The test section is enclosed by an anechoic chamber with the dimension of $3.2 \times 3.1 \times 2\,m^3$.

A circular cylinder was used as the test model in the anechoic wind tunnel. The model has a diameter of $D = 0.064$ m and a length of $L = 0.4$ m, yielding a solid blockage ratio of 16% and an aspect ratio of $L/D = 6.25$. The free-stream velocity U_0 in this experiment ranged from 8 to 35 m s^{-1}, corresponding to diameter-based Reynolds number between 2×10^4 and 1.6×10^5. The convention for the wind tunnel coordinates is defined as follows: The center of the circular cylinder at the mid-span is set as the origin; x represents the streamwise direction; y represents the transverse direction; and z represents the spanwise direction.

B. Surface pattern fabric

As shown in Fig. 2, six surface pattern fabrics, which are labeled as fabrics 3–8, were attached to the circular cylinder. The fabric index follows the definitions in the previous study[6] to make the research consistent. Fabric 3 has thirteen longitudinal grooves distributed on its surface. Fabrics 4 and 5 are characterized by the riblet structures, while fabrics 6 and 7 have structures of convex honeycomb. By contrast, fabric 8 has round surface cavities. These surface structures are evenly distributed on each fabric, forming different types of surface pattern fabric. Moreover, the average surface roughness height for the different surface pattern fabrics was measured by a surface metrology (Bruker NPFLEX). The geometric parameters are summarized in Table I for the reference.

C. Aerodynamic force measurement

A dual-balance setup was used for the force measurement in the anechoic wind tunnel. The JR3 20E12A4-125-EF mFS force balance used in this study has a maximum load range of 40 N in both the x and y directions and a nominal accuracy of $\pm 0.25\%$ within the measurement range. Two force balances connected the ends of the cylinder model to the upper and lower end plates to avoid potential vibration, ensuring that a stationary surface condition was satisfied. The repeatability of the force measurement was evaluated by the seven repeat tests on the smooth cylinder at a Reynolds number of 8.0×10^4. The force measurement has an uncertainty of ± 0.1 N at a level of confidence of 95%. During the tests, the sampling frequency was 5 kHz, and the sampling time was 10 s.

13 January 2025 06:10:20

Published under an exclusive license by AIP Publishing

FIG. 2. Photograph of different surface pattern fabrics wrapped on the cylinder model.

D. Acoustic measurement

As shown in Fig. 3(a), an array of 1/2-in. free-field microphones (G.R.A.S-type 46AE) on a circular arc was placed 1.9 m away from the circular cylinder. The microphone arc array contained seven microphones and allowed observation angle θ_m to range from 40° to 100° in steps of 10°. To record the microphone signals, two 24-bit National Instrument PXIe-4497 cards were used. The sampling frequency was 50 kHz, and the sampling time was 20 s. After the acquisition, fast Fourier transformation was applied to transform the noise data into the frequency domain. The noise data were divided into 39 Hanning windows with 50% overlapping, resulting in a frequency resolution of 2 Hz in the noise spectra. The noise measurement has an uncertainty of ± 0.4 dB at a level of confidence of 95%.

The Amiet's correction method[35] was used to correct the shear layer's rarefaction, as illustrated in Fig. 3(b), where θ_c represents the true directivity angle after corrections. Moreover, the corrections for the sound amplitude can be ignored, as the cylinder flow is within the low-Mach number range.[35]

TABLE I. Geometric parameters of the surface pattern fabrics.

Fabric index	$R_a(\mu m)$	Surface pattern
3	156.5	Grooves
4	254.4	Riblets
5	275.5	Riblets
6	301.2	Convex honeycomb
7	531.2	Convex honeycomb
8	827.4	Round cavities

E. Hot-wire measurement

A Dantec CTA 55P11 single-sensor hot-wire probe and a Dantec StreamLine Pro Anemometer system were used for the flow measurement. The probe was calibrated by the Dantec StreamLine Pro Automatic Calibrator within a speed range between 5 and 40 m s^{-1} before the measurement. During the test, the motion of the probe was precisely controlled by a 3D transverse system with a spatial resolution

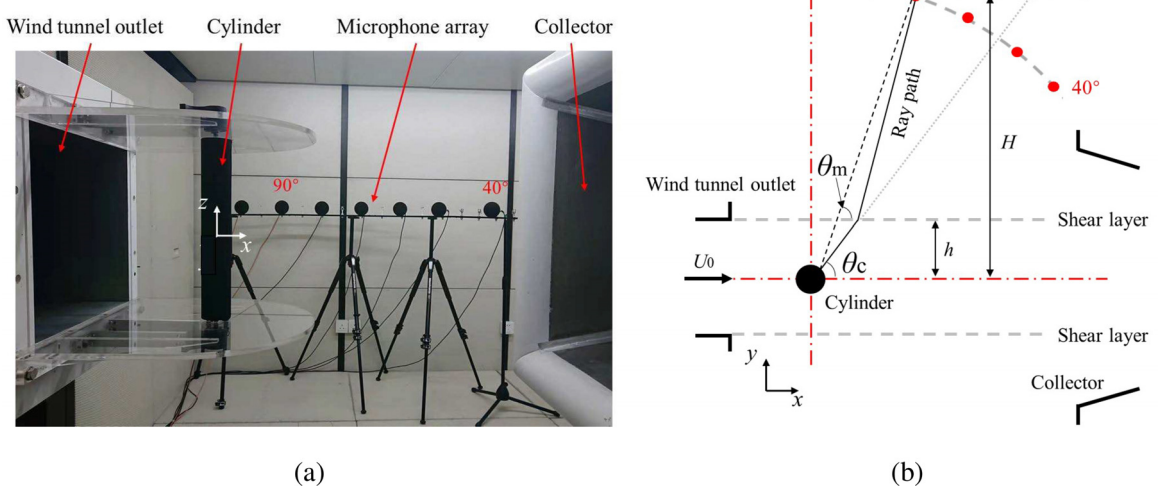

(a) (b)

FIG. 3. The experiment setup of the cylinder noise measurement: (a) the experiment setup of the noise directivity measurement and (b) top schematic of the noise directivity measurement, including the ray path of the cylinder noise due to the shear layer rarefaction.

13 January 2025 06:10:20

Published under an exclusive license by AIP Publishing

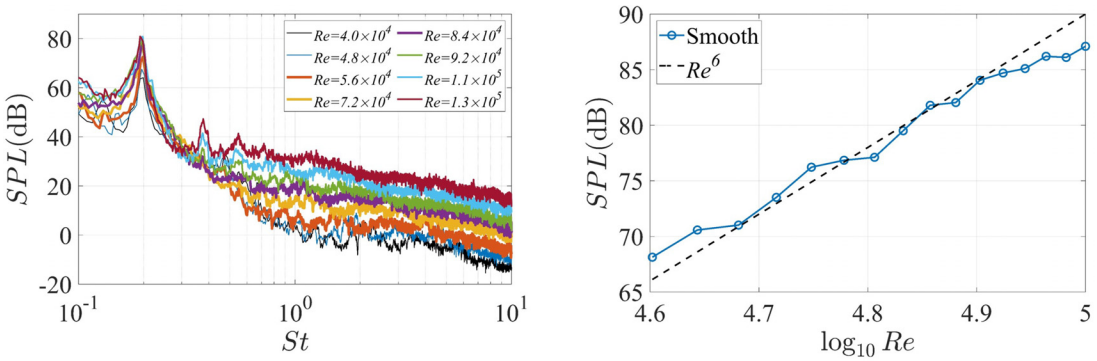

FIG. 4. The noise measurement results for the smooth cylinder: (a) the sound spectra at different Reynolds numbers and (b) variation of the Aeolian tone intensity with *Re*. Bandwidth: 1/3 octave.

of 0.01 mm. The hot-wire probe scanned the cylinder wake at locations of $x/D = 2$ and $-1.25D \le y \le 1.25D$ with a step of $y/D = 0.16$. All the measurement stations are located at $z = 0$. For each measurement, the sampling frequency and time for the hot-wire measurements were 20 kHz and 10 s, respectively. After the acquisition, temperature correction[36] was applied to compensate for the rise in the temperature inside the wind tunnel.

III. RESULTS AND DISCUSSION

A. Smooth cylinder

1. Force and noise measurement

The results for the smooth cylinder are first discussed to provide a benchmark case and validate the conditions of the anechoic wind tunnel tests. For the results at 90° microphone location, Fig. 4(a) shows the noise spectra for the smooth cylinder at various Reynolds numbers ($Re = U_0 D/\nu$, where ν is the kinematic viscosity). A clear phenomenon is that significant peaks appear at Strouhal number ($St = fD/U$) of about 0.19, which are mainly caused by the regular vortex shedding in the sub-critical regime.

As shown in Fig. 4(b), the variations of the peak amplitude, which is calculated from the noise spectra with a 1/3 octave range, are also evaluated at different Reynolds numbers. The results closely follow the sixth power of *Re*, suggesting that the far-field condition is satisfied under the current experiment setup.[37] Therefore, the overall sound pressure level (*OASPL*) can be normalized by the six power of U_0 for a fair comparison between different Reynolds numbers. The normalized *OASPL*, denoted by $OASPL^*$, can be computed as

$$OASPL^* = OASPL - 10\log_{10}\left(U_0^6\right), \tag{1}$$

where *OASPL* accounts for frequencies between 15 Hz and 20 kHz.

Figure 5 shows the force coefficients and $OASPL^*$ for the smooth cylinder at Reynolds numbers from 4.0×10^4 to 1.4×10^5. In this study, the drag coefficient C_d is defined as $C_d = 2F_d/\rho U_0^2 DL$, where F_d is the mean drag force, and ρ is the air density. The lift fluctuation coefficient C_l' and the drag fluctuation coefficient C_d' are defined as $C_l' = 2F_l'/\rho U_0^2 DL$ and $C_d' = 2F_d'/\rho U_0^2 DL$, respectively, where F_l' is root mean square (RMS) of the lift fluctuation force, and F_d' is RMS of the drag fluctuation force. In the measured Reynolds number range, C_D keeps almost constant at a value of about 1.1, which suggests that the cylinder flow is within the sub-critical regime.[5] The C_l' and C_d' also stay nearly constant in the sub-critical regime, but the values of C_d' are rather small compared to those of C_l', suggesting that the fluctuating force on the cylinder is mainly along the transverse direction (*y*-axis). Since the C_l' is the key factor that determines the cylinder noise level,[37] the variations of $OASPL^*$ for the smooth cylinder are insignificant (within 5 dB). However, the $OASPL^*$ has a continuous drop, which is probably influenced by the reduced coherent length of pressure fluctuations at higher Reynolds numbers.[38]

Figure 6 shows the noise directivity for the smooth cylinder. Since the acoustic dipole is characterized by two lobes with equal noise radiation forward and backward, the noise directivity for the smooth cylinder shows typical dipole features, where the *OASPL* around $\theta_m = 90°$ reaches the maximum value. The results at higher Reynolds number also represent similar directivity patterns but with increased amplitudes. The noise directivity measurement can also be validated by comparing it with the theoretical noise directivity. Based on the function for the cylinder noise,[37] the theoretical noise directivity can

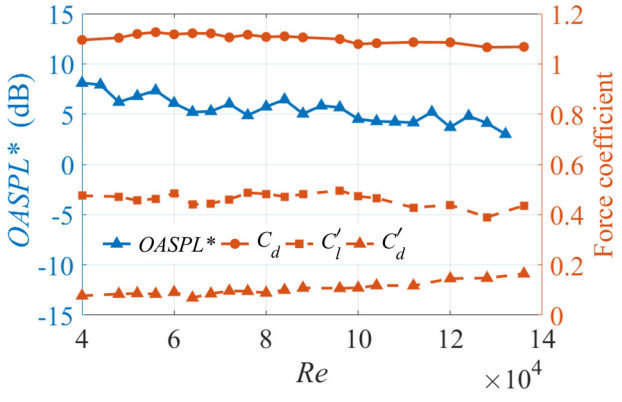

FIG. 5. The measurement results of C_d, C_d', C_l', and $OASPL^*$ for the smooth cylinder at different *Re* values.

13 January 2025 06:10:20

Published under an exclusive license by AIP Publishing

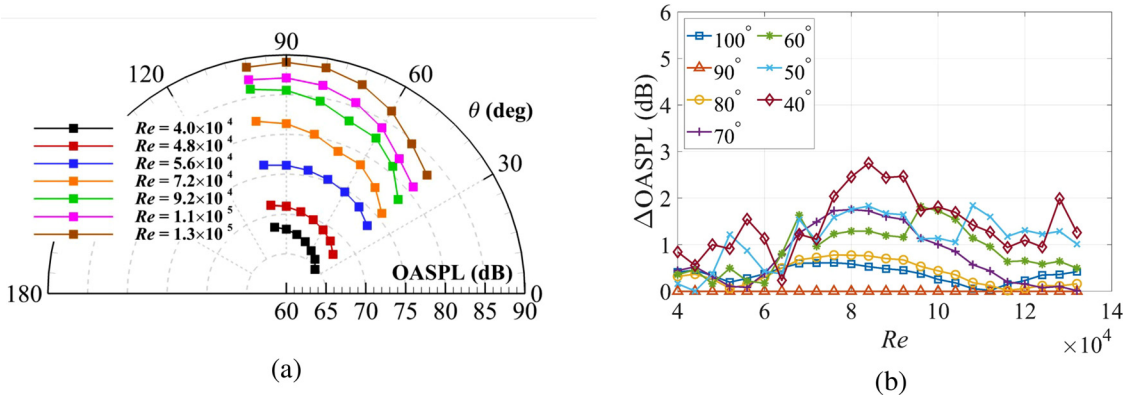

FIG. 6. (a) Noise directivity of the smooth cylinder in the sub-critical regime. (b) Experimental deviations from the theoretical directivity.

be described by the difference of *OASPL* between 90° and other observation angles,

$$OASPL_{90^\circ} - OASPL_{\theta_c} = 10\log_{10}\left(\frac{\sin^2\theta_c}{(1+M\cos\theta_c)^4}\right), \quad (2)$$

where M is the Mach number.

Deviations in the experiment ($\Delta OASPL$) can be evaluated by the differences between $OASPL_{90^\circ} - OASPL_{\theta_m}$ for the experiment and $OASPL_{90^\circ} - OASPL_{\theta_c}$ for the theory. Figure 6(b) shows the results in terms of $\Delta OASPL$ at each θ_m. Except for the results at 40° microphone location, good agreement between the experiment results and theoretic predictions is achieved with the maximum $\Delta OASPL$ less than 2 dB. As identified by the previous studies,[39,40] the existence of the wind tunnel collector may generate additional noise identified as the turbulent boundary layer noise and the vortex interaction noise. Since the 40° microphone is located near the wind tunnel collector, the accuracy of the noise measurement may be vulnerable to the additional noise or the enhanced sound scattering effects, by which the 40° microphone shows larger measurement uncertainty.

B. Cylinder with surface pattern fabrics

1. Force and noise measurement results

Figure 7 shows the drag and noise measurement results for the cylinder with different surface pattern fabrics. Compared to the results of the smooth cylinder in Fig. 5, different surface pattern fabrics significantly reduce drag and noise simultaneously but in different *Re* ranges. It is clear that variations of C_d for different surface pattern fabrics show common features in each flow regime. In the sub-critical regime, C_d is nearly constant at a value of about 1.2. With the increase in *Re*, C_d experiences sudden and continuous drops to a minimum value of about 0.6, which corresponds to about 50% drag reductions compared to that for the smooth cylinder. The substantial reductions in C_d are referred to as drag crisis,[41] representing the cylinder flow in the critical regime. After reaching the minimum value, C_d increases again in the supercritical regime. Based on the changes in C_d, the Reynolds number ranges for the critical flow regime are estimated and summarized in Table II, facilitating the following discussions. Unlike the influence of surface roughness on the critical Reynolds number,[15] the decrease in the critical Reynolds number for the cylinder with surface pattern fabrics does not vary with an increase in R_a alone, suggesting that the shapes of surface patterns have significant impacts on the flow transitions, and thus the critical Reynolds number ranges.

Moreover, variations of $OASPL^*$ at 90° microphone location have the same tendency as that of C_d, suggesting that the noise attenuation and the drag reduction are highly correlated. In particular, the maximum drag and noise reductions can be achieved at the same time, as the minimum C_d and the minimum $OASPL^*$ share almost the same *Re*.

In terms of force fluctuations, the overall values of C_l' are much larger than those for C_d', suggesting that C_l' mainly contributes to the dipole noise.[38] In the critical regime, C_l' has a continuous drop, corresponding to the decreases in $OASPL^*$. After reaching the minimum point, C_l' rises again in the supercritical regime, which is mainly responsible for the increased $OASPL^*$ in this flow regime. In brief, the variations of C_l' are mainly responsible for the changes in $OASPL^*$ in each flow regime, which is also in accordance with the formula of the theoretical Aeolian tone intensity[29,37] as C_l' is the main influencing parameter for the cylinder noise.

2. Comparison of the acoustic spectra

Figure 8 shows the noise spectra for different surface pattern fabrics to explore the direct reasons behind the noise reductions. For the cylinder flow in each regime, the noise spectra for different surface pattern fabrics show similar characteristics. In the sub-critical regime, the Aeolian tones have clear peaks at $St \approx 0.19$, corresponding to the generations of high lift fluctuation coefficients in Fig. 7. Moreover, their peak amplitudes are close to those for the smooth cylinder in the sub-critical regime, showing that the surface pattern fabrics have little influence on the noise spectra in the sub-critical regime.

In the critical regime, the peak amplitudes are gradually reduced at higher Reynolds numbers, which is associated with the decreased lift fluctuation coefficients. Meanwhile, the peak moves toward higher Strouhal numbers (over 0.2). At the end of the critical regime, there are wide humps rather than clear peaks, suggesting that the noise is mainly broadband, which leads to significant reductions in $OASPL^*$ (see Fig. 7).

13 January 2025 06:10:20

Published under an exclusive license by AIP Publishing

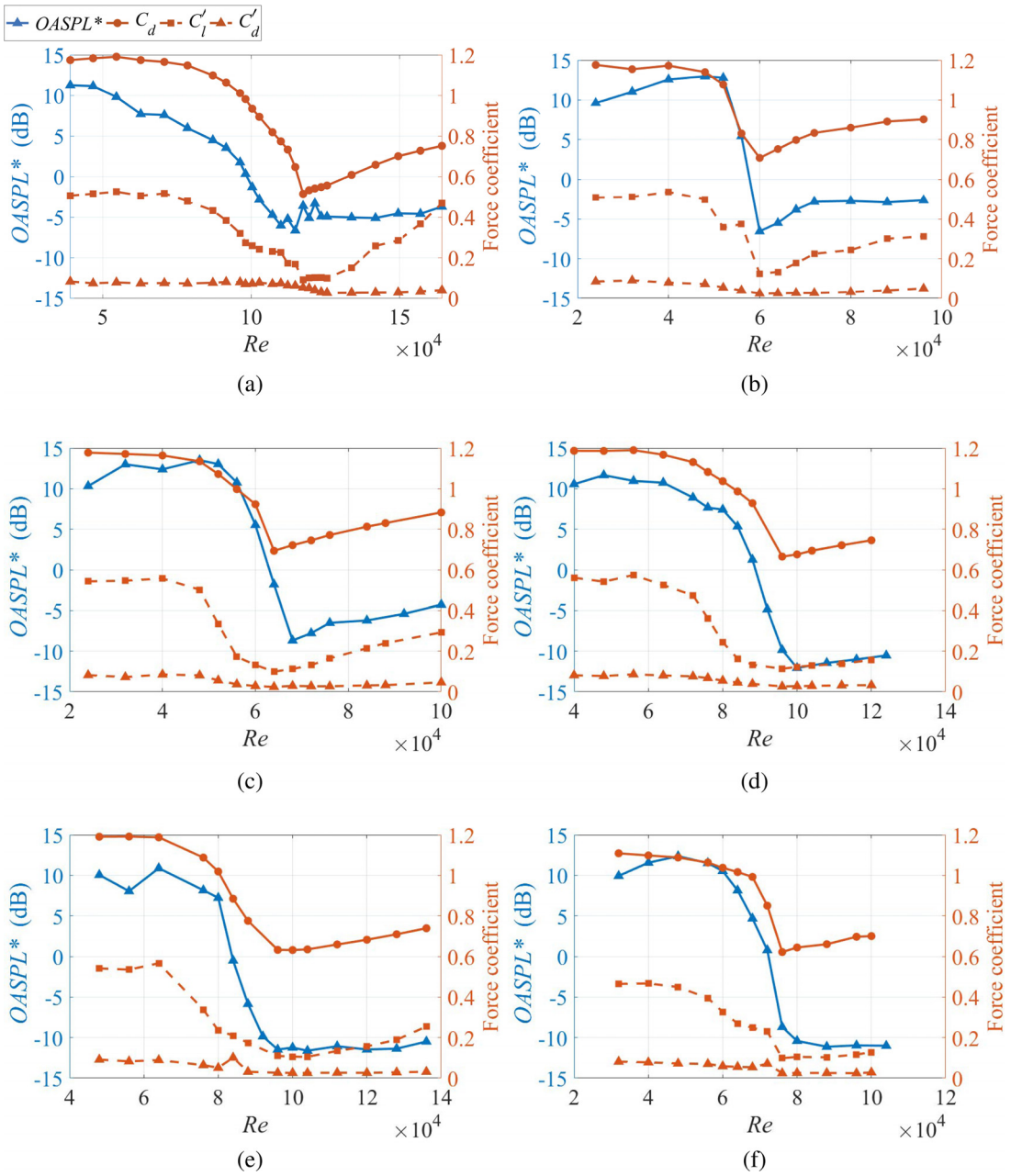

FIG. 7. The measurement results of C_d, C_d', C_l', and $OASPL^*$ for the cylinder with fabrics 3–8 at different *Re* values. (a) Fabric 3, (b) Fabric 4, (c) Fabric 5, (d) Fabric 6, (e) Fabric 7, and (f) Fabric 8.

TABLE II. Critical Reynolds number ranges for surface pattern fabrics.

Index	Fabric 3	Fabric 4	Fabric 5
Re	$[6.9 \times 10^4, 1.18 \times 10^5]$	$[5.2 \times 10^4, 8.0 \times 10^4]$	$[4.8 \times 10^4, 6.8 \times 10^4]$
Index	Fabric 6	Fabric 7	Fabric 8
Re	$[7.2 \times 10^4, 1.00 \times 10^5]$	$[6.4 \times 10^4, 9.6 \times 10^4]$	$[4.8 \times 10^4, 8.0 \times 10^4]$

13 January 2025 06:10:20

Published under an exclusive license by AIP Publishing

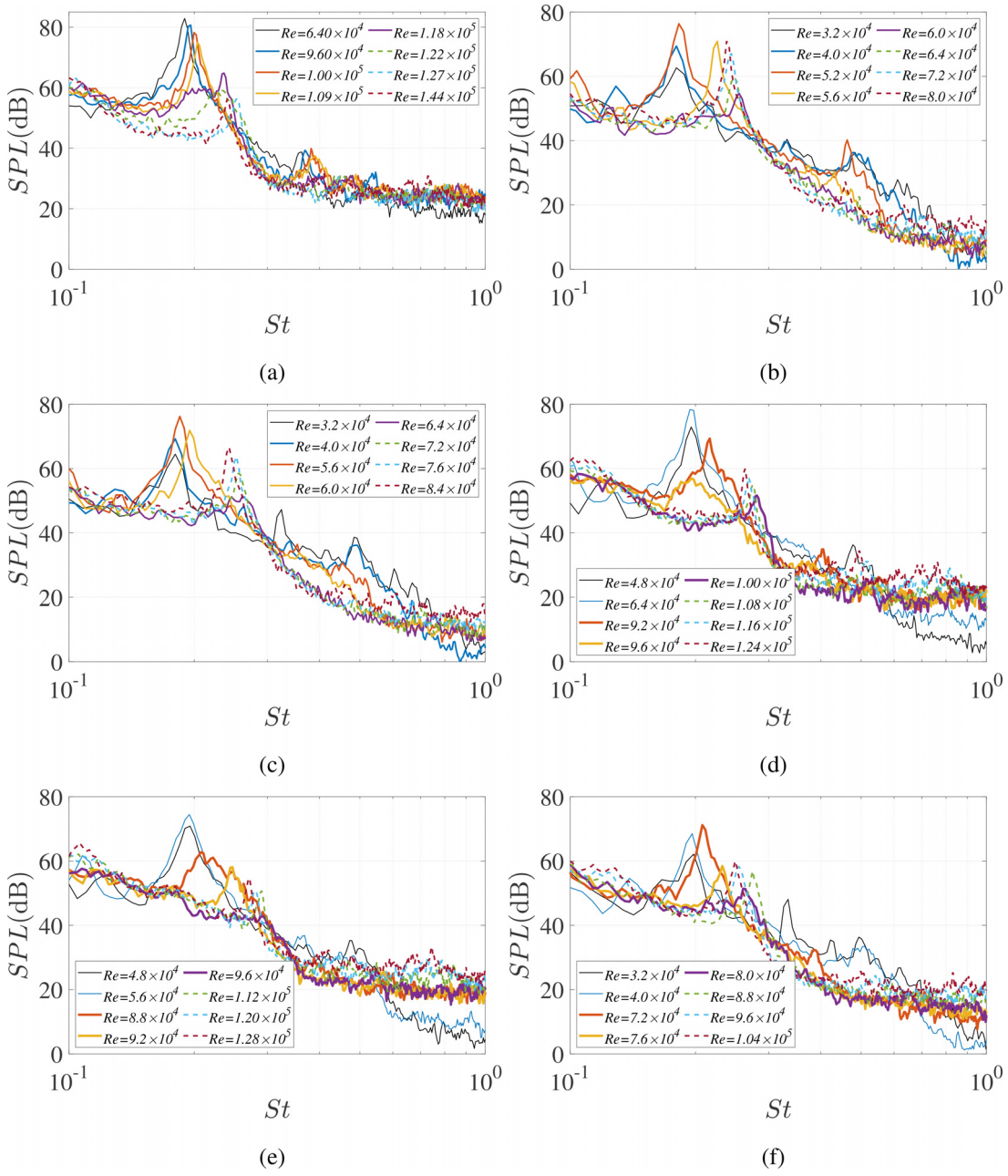

FIG. 8. Comparison of noise spectra for the cylinder with surface pattern fabrics. Here, the solid, bold solid, and dashed lines represent the cylinder flow in the sub-critical, critical, and supercritical regimes, respectively. (a) Fabric 3, (b) Fabric 4, (c) Fabric 5, (d) Fabric 6, (e) Fabric 7, and (f) Fabric 8.

In the supercritical regime, the Aeolian tones reappear again at St near 0.3 but with low amplitude, suggesting the regeneration of the vortex shedding with weak strength. The peak amplitudes increase at higher Reynolds numbers, which is the direct reason for the increase in $OASPL^*$ and corresponds to the rise in C_l'. However, the peak amplitudes are still much lower than those in the sub-critical regime, which explains the relatively low values of $OASPL^*$ in this flow regime.

The Strouhal numbers of the Aeolian tones for different surface pattern fabrics show the similar trend in the corresponding flow regimes. In the sub-critical regime, the peaks are located at $St \approx 0.19$, identical to that for the smooth cylinder. In the critical regime, the

13 January 2025 06:10:20

Published under an exclusive license by AIP Publishing

Strouhal numbers increase at higher Reynolds number and reach a maximum value above 0.2 before the disappearance of the peak. As identified by the previous study, the rise in St is associated with the drop in C_D (Fig. 7). The delay of the flow separation and, thus, the shorter distance between the separated shear layers change the double-shear-layer instability,[41] by which the Strouhal number increases.[5,16] In the supercritical regime, the Aeolian tone reappears at higher Strouhal numbers of about 0.25. With the increase in the Reynolds number, the Strouhal number of the Aeolian tones experiences a continuous drop, which matches the rise in C_D in the supercritical regime. It is also noted that the change of the Strouhal number is comparable to that for a smooth cylinder in the critical and supercritical flow regimes,[7,42] showing that the flow mechanism in each flow regime is similar.

3. Comparison of the acoustic directivities

The noise directivities for the cylinder with different surface fabrics are compared in Fig. 9. In the sub-critical regime, the noise directivity shows clear dipole patterns, where the *OASPL* around 90° has the maximum value. Since the values of C_l' remain constant in the sub-critical regime, the surface pattern fabrics have little influence on the noise directivity in the sub-critical regime.

In the critical regime, the noise directivities gradually lose their dipole characteristics, where the differences between the *OASPL* at 90° and other angles become less. This phenomenon is associated with the significant drop in C_l' in the critical regime, by which C_l' and C_d' have closed values and, thus, the contributions of C_d' to the sound fields cannot be ignored. Moreover, noise reductions are observed for all the

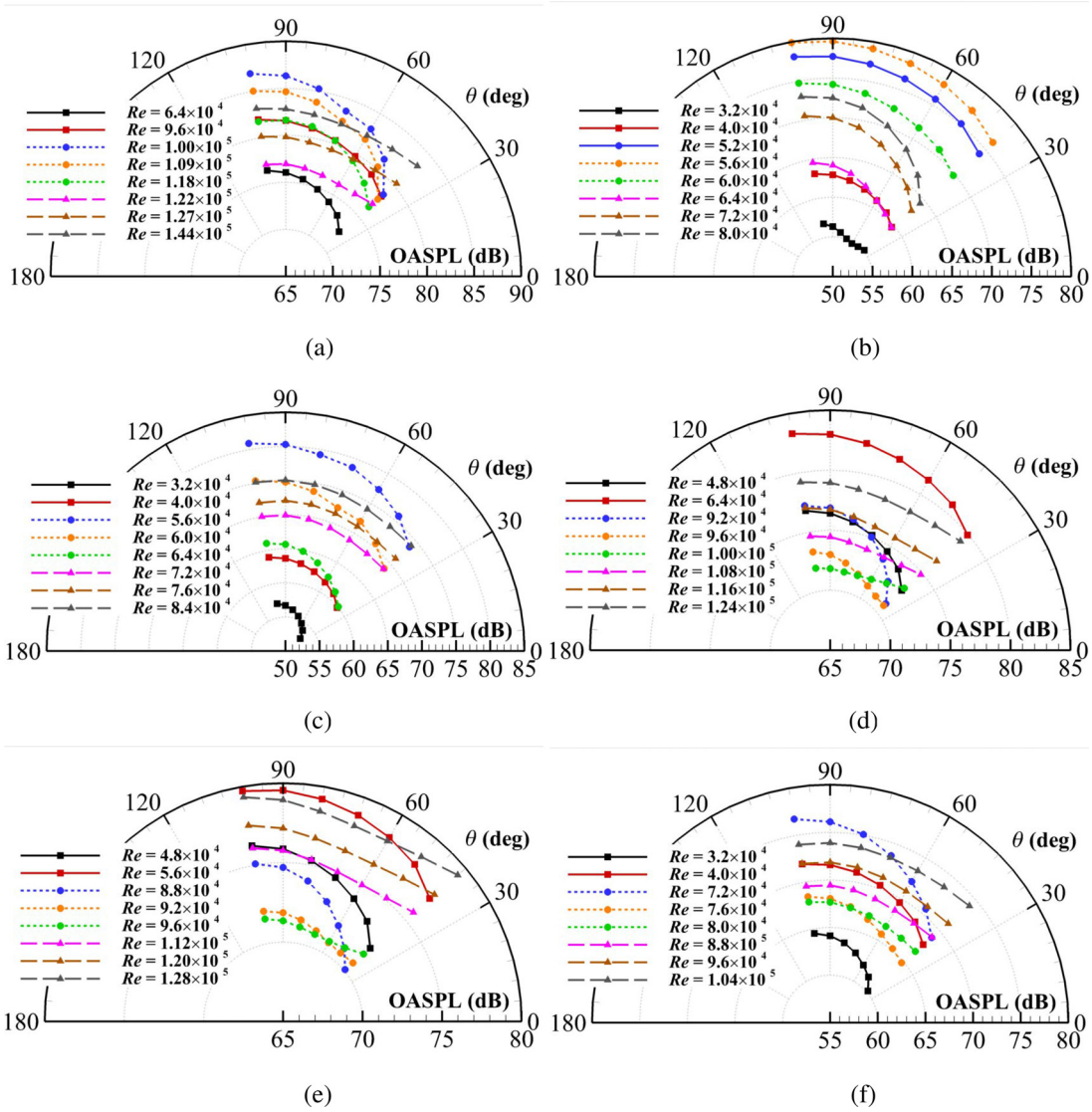

FIG. 9. Comparison of noise directivity for the cylinder with surface pattern fabrics in different flow regimes. Here, the solid, dotted, and dashed lines represent the cylinder flow in the sub-critical, critical, and supercritical regimes, respectively. (a) Fabric 3, (b) Fabric 4, (c) Fabric 5, (d) Fabric 6, (e) Fabric 7, and (f) Fabric 8.

13 January 2025 06:10:20

Published under an exclusive license by AIP Publishing

radiation angles. For example, fabric 5 reduces the *OASPL* up to 15 dB from $Re = 5.6 \times 10^4$ to 6.4×10^4 at all the observation angles. In general, these results reveal that the noise reductions for different surface pattern fabrics are significant in the critical regime for all the observation angles.

In the supercritical regime, the *OASPL* is increased at higher Reynolds numbers, which is associated with the rise in C_l' (Fig. 8). The noise directivity for different surface pattern fabrics tends to be uniform at different angles. Previous studies have shown that the fluctuating lift on the cylinder surface has spanwise segments in the supercritical regime.[29,43] The segment depends on the degree of three dimensionality in the vortex shedding, which also has a great influence on the Aeolian tone.[43] It is assumed that the spanwise segment of lift fluctuations causes the sound source along the spanwise direction of the cylinder to be out of phase. Considering each lift fluctuation segment as a dipole sound source, the far-field noise can be affected by the effects of destructive interference at the microphone locations.[44] For this reason, the noise directivity in the supercritical regime loses its dipole features. It also suggests that surface pattern fabrics reduce cylinder noise not only by reducing lift fluctuations but also by relying on reducing spanwise coherence, causing the sound pressure to have destructive interferences at the far-field locations.

Figure 10 shows the variations of the Aeolian tone intensity for the cylinder with fabric 3 at different Reynolds numbers. In the sub-critical flow regime, the Aeolian tones follow the sixth-power law scaling with the Reynolds number, which suggests the aerodynamic dipole type of the cylinder noise. In the critical regime, the Aeolian tone intensities showed a dramatic drop with an increase in the Reynolds number, which does not follow the sixth-power law of the Reynolds number. In the supercritical regime, although the Aeolian tone intensity increases again, its variations also do not increase, which is in accordance with the sixth-power law of the Reynolds number. For this reason, the cylinder noise in the critical and supercritical regimes may not have the characteristics of a dipole noise source, and the noise directivity for the cylinder with fabric 3 becomes gradually omnidirectional [Fig. 9(a)]. Moreover, as the classification of the flow regimes is determined by flow states, e.g., laminar or turbulent, it is assumed that the loss of the dipole features is associated with the phenomenon of the boundary layer transition at different Reynolds numbers, by which the cylinder noise in different flow regimes exhibits different characteristics.

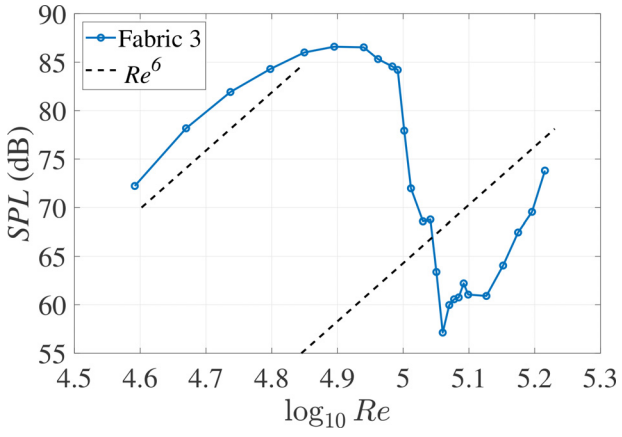

FIG. 10. Variations of the Aeolian tone intensity (90° microphone) for the cylinder with fabric 3 at different Reynolds numbers.

C. Near-wake flow measurement

In this section, the cylinder flow is analyzed to further reveal the roles of surface pattern fabric on drag and noise reductions. As the aerodynamic and aeroacoustic characteristics of the cylinder with surface pattern fabrics show similarities in the corresponding flow regime, the flow data for the cylinder with fabric 3 were analyzed to show the general flow features.

Figure 11 shows the mean velocity profiles (U) of the cylinder with fabric 3 at $x/D = 2$. Starting at the critical regime, the wakes become apparently narrowed, and the minimum velocity is reduced at higher Reynolds numbers, which indicates that the flow separation was delayed downstream. For this reason, the drag coefficient has a continuous drop in this regime. It is assumed that the surface patterns on fabric 3 produce vortices (disturbances) in the boundary layer and thus, strong near-wall momentum is generated through mixing enhancement. This phenomenon transports kinetic energy from the edge of the boundary layer to the low-momentum flow near the cylinder surface, preventing the separation that would occur for a laminar boundary layer at the same Reynolds number. Therefore, the drag crisis for the cylinder with fabric 3 occurs at lower Reynolds numbers, compared to that of the smooth cylinder.[5] With the increase in the Reynolds number in the critical regime, the momentum mixing is enhanced, resulting in continuous drop in C_D in Fig. 7(a). For this reason, the Reynolds number effects of different surface pattern fabrics suggest that vortices (disturbances) produced over them are varied, which contributes to the different degrees of momentum mixing and thus the occurrence of the drag crisis in different Reynolds number ranges. It is noticeable that the wake becomes clearly asymmetric at $Re = 1.18 \times 10^5$. This wake behavior is probably caused by the appearance of separation bubbles (flow separation and the following flow attachment) on a single side of the cylinder, which leads to a significant downstream shift of the flow separation on this side, and thus the asymmetric cylinder wake. In comparison, the wake in the supercritical regime ($Re = 1.22 \times 10^5$ and 1.27×10^5) becomes symmetric again, partly because the separation bubble disappears, and the flow becomes fully turbulent before the main separation. Meanwhile, the

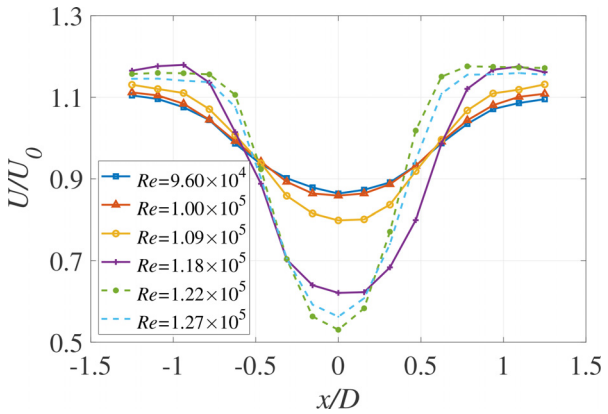

FIG. 11. Velocity profiles of the cylinder with fabric 3.

13 January 2025 06:10:20

Published under an exclusive license by AIP Publishing

C_D only has relatively small variations [Fig. 7(a)], which further indicates that the boundary layer flow becomes fully turbulent on each side of the cylinder in the supercritical regime.

We further reveal the unsteady wake behaviors by performing the wavelet analysis[45] on the hot-wire data at the location of $y/D = -0.63$ and $x/D = 2$. Figure 12 shows the wavelet maps represented by the normalized wavelet energy as $u/(U_0D)$ (u is the velocity fluctuations). A threshold of 1.7 was set in the wavelet maps to isolate the dominant energy.

At the beginning of the critical regime ($Re = 9.60 \times 10^4$), the wavelet energy concentrates at $St \approx 0.19$, exhibiting the typical shedding motions of Kármán vortices. In addition, the value of St for the

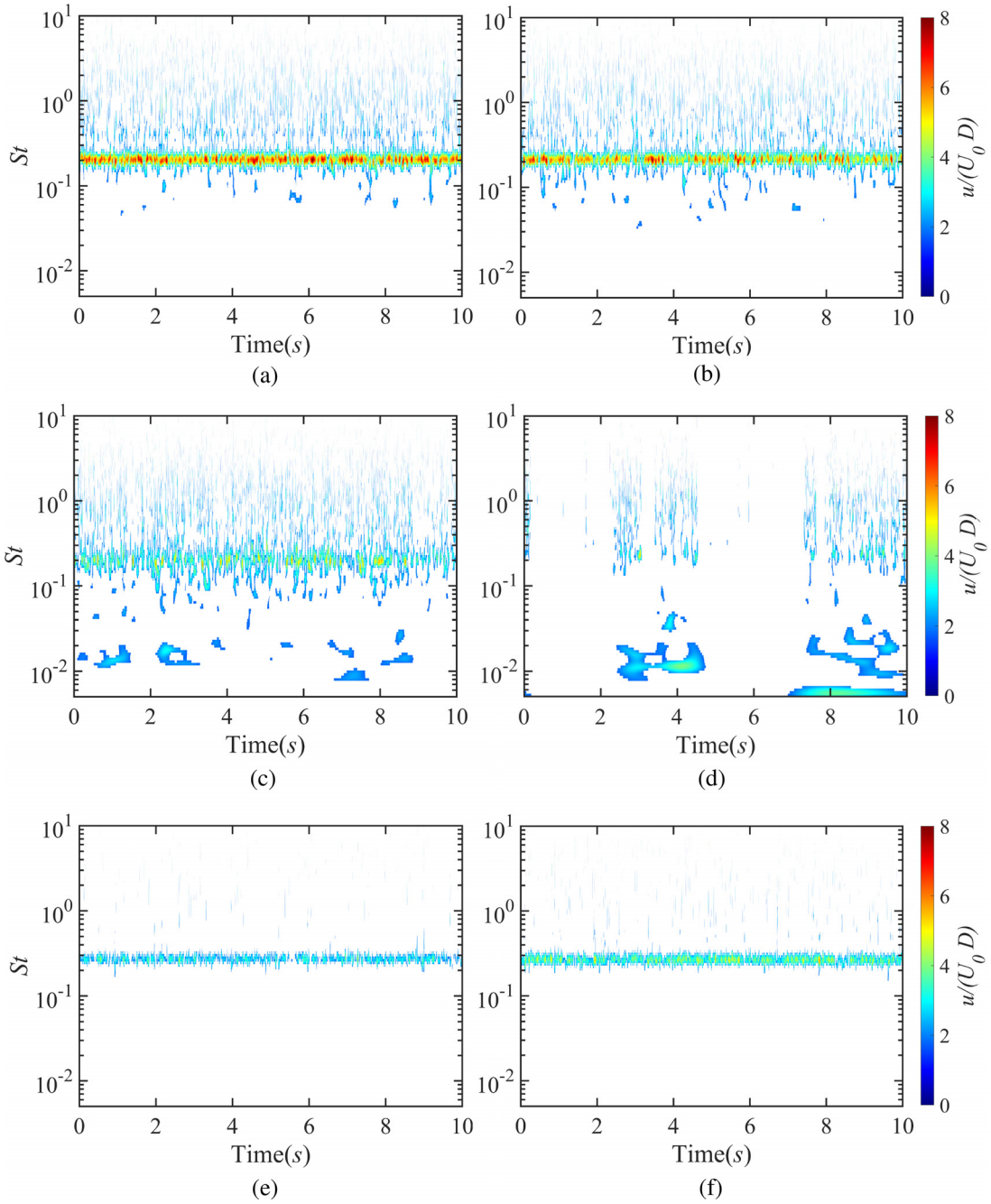

FIG. 12. The results of wavelet analysis for the cylinder with fabric 3 at the location of $y/D = -0.63$ and $x/D = 2$: (a) $Re = 9.60 \times 10^4$; (b) $Re = 1.00 \times 10^5$; (c) $Re = 1.09 \times 10^5$; (d) $Re = 1.18 \times 10^4$; (e) $Re = 1.22 \times 10^4$; and (f) $Re = 1.27 \times 10^4$.

13 January 2025 06:10:20

Published under an exclusive license by AIP Publishing

vortex shedding is identical to that for the Aeolian tones (Fig. 8 shows that the Aeolian tone is mainly caused by the vortex shedding). At higher Reynolds numbers, Figs. 12(b) and 12(c) reveal more intricate flow dynamics with intermittent and irregular energy distributions at low frequencies. The vortex shedding (wavelet energy at $St \approx 0.19$) becomes even less energetic, corresponding to reduced lift fluctuations and the suppression of the Aeolian tone in the critical regime [Figs. 7(a) and 8(a)]. The weak vortex shedding is probably associated with the three-dimensional vortex dynamics,[7,46] which leads to the spanwise segments of the sound sources along the cylinder surface, and thus the noise reductions [Fig. 7(a)]. At the end of the critical regime, Fig. 12(d) shows that the wavelet energy for vortex shedding becomes even low, whereas the intermittent low-frequency energy components become dominant. This intermittent feature provides evidence for the existence of the separation bubble, as its partial reattachment is characterized by pulsating features with low frequencies.[42,47] Furthermore, the emergence of the separation bubble on one side of the cylinder further breaks the two-shear-layers instability of the cylinder flow,[41] causing the almost total suppression of the regular vortex shedding. As a result, when the separation bubble appears, fabric 3 on the cylinder can achieve the maximum noise reduction [Fig. 7(a) at $Re = 1.18 \times 10^4$].

Figures 12(e) and 12(f) reveal the wavelet map in the supercritical regime. Unlike the flow in the critical regime, continuous and concentrated vortex shedding energy reappears at higher Strouhal numbers ($St \approx 0.3$) which are in accordance with St of the Aeolian tone. This result shows that the regeneration of the regular vortex shedding is the main reason that the Aeolian tones reappear in the noise spectra [Fig. 8(a)] at higher Strouhal numbers. However, the amplitudes of the wavelet energy of the vortex shedding are still relatively low, which also explains the small Aeolian peaks, and thus the small values of $OASPL^*$ in the supercritical regime (Fig. 7).

IV. CONCLUSIONS

Through the anechoic wind tunnel tests, we investigated the effects of six surface pattern fabrics on the noise and drag reductions on a circular cylinder. The results show that different surface pattern fabrics reduce noise and drag simultaneously but in different Reynolds number ranges. The aerodynamic and aeroacoustic characteristics of the cylinder with different surface pattern fabrics show similarities corresponding to the cylinder flow in different flow regimes.

In the sub-critical regime, the overall values of the lift fluctuation coefficient are much larger than the drag fluctuation coefficient, by which the noise directivity for the cylinder with different surface pattern fabrics shows typical dipole features. The higher lift fluctuation coefficient is also associated with the clear Aeolian tones located at a Strouhal number of about 0.19. The hot-wire measurement further reveals that the clear Aeolian tone is mainly caused by the regular vortex shedding at the same Strouhal number (about 0.19).

In the critical regime, the surface pattern fabrics simultaneously reduce cylinder drag and noise. The drag reduction is because the surface pattern fabric can delay the flow separation, resulting in narrowed wakes in the critical and supercritical regimes. The suppression of the Aeolian tones in the critical regime is the direct reason for the cylinder noise reductions, which is also associated with the reduced lift fluctuation coefficients. Especially, the noise directivity gradually loses its dipole characteristics, which is probably related to the reduced lift fluctuating force and the three-dimensional wake dynamics. Based on the wavelet analysis, the vortex shedding gradually loses its strength in the critical regime, which explains the suppression of the Aeolian tones, and thus the noise reductions. In particular, the random low-frequency energy components shown in the wavelet energy map provide evidence for the formation of separation bubbles in the critical regime. When the separation bubble appears, these low-frequency components become dominant, and vortex shedding is almost ceased, which explains the lowest cylinder noise that happened at this stage.

In the supercritical regime, the drag and noise show a slightly upward trend. The direct reason is the reappearance of the Aeolian tones and the increased lift fluctuation coefficients. However, compared to the Aeolian tone intensity in the sub-critical regime, the peak amplitudes are still low, which explains the low noise levels. The noise directivity becomes uniform at different radiation angles, which may be caused by the spanwise segments of the dipole sound sources. In addition, the reappearance of the regular vortex shedding in the wake explains the regeneration of the Aeolian tones, and the low vortex shedding strength is the reason for the low Aeolian tone intensity.

The results revealed in this study are significant, as the critical Reynolds number ranges can be controlled by changing different surface patterns on a piece of fabric. In the future, different surface pattern fabrics can be applied to maximize noise and drag reductions in engineering applications where the Reynolds number effects are dominant, e.g., drag reductions on a cyclist.

ACKNOWLEDGMENTS

This work was partially supported by the Hong Kong Innovation and Technology Commission (Grant No. ITS/354/18FP) and the A. Kwok Sports Aerodynamics Science Initiative. We also would like to thank the Hong Kong Sports Institute for the support of this work. The study was conducted in the Aerodynamics Acoustics & Noise Control Technology Centre (AANTC) at the Hong Kong University of Science and Technology (http://aantc.ust.hk).

AUTHOR DECLARATIONS

Conflict of Interest

The authors have no conflicts to disclose.

Author Contributions

Chuntai Zheng: Conceptualization (equal); Data curation (equal); Formal analysis (equal); Methodology (equal); Writing – original draft (equal). **Peng Zhou:** Investigation (equal); Writing – review & editing (equal). **Siyang Zhong:** Supervision (equal); Writing – review & editing (equal). **Xin Zhang:** Conceptualization (equal); Methodology (equal); Project administration (equal); Resources (equal); Supervision (equal); Writing – review & editing (equal).

DATA AVAILABILITY

The data that support the findings of this study are available from the corresponding author upon reasonable request.

REFERENCES

[1]H. Choi, W.-P. Jeon, and J. Kim, "Control of flow over a bluff body," Annu. Rev. Fluid Mech. **40**, 113–139 (2008).

13 January 2025 06:10:20

Published under an exclusive license by AIP Publishing

[2]T. N. Crouch, D. Burton, Z. A. LaBry, and K. B. Blair, "Riding against the wind: A review of competition cycling aerodynamics," Sports Eng. **20**, 81–110 (2017).
[3]T. Sueki, M. Ikeda, and T. Takaishi, "Aerodynamic noise reduction using porous materials and their application to high-speed pantographs," Q. Rep. RTRI **50**(1), 26–31 (2009).
[4]K. Chode, H. Viswanathan, and K. Chow, "Noise emitted from a generic side-view mirror with different aspect ratios and inclinations," Phys. Fluids **33**(8), 084105 (2021).
[5]M. M. Zdravkovich, *Flow around Circular Cylinders: Volume 2: Applications* (Oxford University Press, 1997), Vol. 2.
[6]C. Zheng, P. Zhou, S. Zhong, X. Zhang, X. Huang, and R. C.-H. So, "An experimental investigation of drag and noise reduction from a circular cylinder using longitudinal grooves," Phys. Fluids **33**(11), 115110 (2021).
[7]E. Achenbach and E. Heinecke, "On vortex shedding from smooth and rough cylinders in the range of Reynolds numbers 6×10^3 to 5×10^6," J. Fluid Mech. **109**, 239–251 (1981).
[8]O. Güven, C. Farell, and V. C. Patel, "Surface-roughness effects on the mean flow past circular cylinders," J. Fluid Mech. **98**(4), 673–701 (1980).
[9]L. Oggiano, O. Troynikov, I. Konopov, A. Subic, and F. Alam, "Aerodynamic behaviour of single sport jersey fabrics with different roughness and cover factors," Sports Eng. **12**(1), 1–12 (2009).
[10]Y. Z. Liu, L. L. Shi, and J. Yu, "Tr-PIV measurement of the wake behind a grooved cylinder at low Reynolds number," J. Fluids Struct. **27**(3), 394–407 (2011).
[11]Y. Yamagishi and M. Oki, "Effect of groove shape on flow characteristics around a circular cylinder with grooves," J. Visualization **7**(3), 209–216 (2004).
[12]B. Zhou, X. Wang, W. Guo, W. M. Gho, and S. K. Tan, "Experimental study on flow past a circular cylinder with rough surface," Ocean Eng. **109**, 7–13 (2015).
[13]P. Bearman and J. Harvey, "Control of circular cylinder flow by the use of dimples," AIAA J. **31**(10), 1753–1756 (1993).
[14]S. Huang, "VIV suppression of a two-degree-of-freedom circular cylinder and drag reduction of a fixed circular cylinder by the use of helical grooves," J. Fluids Struct. **27**(7), 1124–1133 (2011).
[15]E. Achenbach, "Influence of surface roughness on the cross-flow around a circular cylinder," J. Fluid Mech. **46**(2), 321–335 (1971).
[16]P. W. Bearman, "On vortex shedding from a circular cylinder in the critical Reynolds number regime," J. Fluid Mech. **37**(3), 577–585 (1969).
[17]E. Achenbach, "Distribution of local pressure and skin friction around a circular cylinder in cross-flow up to re= 5×10^6," J. Fluid Mech. **34**(4), 625–639 (1968).
[18]A. Roshko, "Experiments on the flow past a circular cylinder at very high Reynolds number," J. Fluid Mech. **10**(3), 345–356 (1961).
[19]G. Schewe, "On the force fluctuations acting on a circular cylinder in crossflow from subcritical up to transcritical Reynolds numbers," J. Fluid Mech. **133**, 265–285 (1983).
[20]T. F. Geyer and E. Sarradj, "Circular cylinders with soft porous cover for flow noise reduction," Exp. Fluids **57**(3), 1–16 (2016).
[21]S. A. Showkat Ali, X. Liu, and M. Azarpeyvand, "Bluff body flow and noise control using porous media," AIAA Paper No. 2016-2754, 2016.
[22]T. Sueki, T. Takaishi, M. Ikeda, and N. Arai, "Application of porous material to reduce aerodynamic sound from bluff bodies," Fluid Dyn. Res. **42**(1), 015004 (2010).
[23]H. Du, Q. Zhang, Q. Li, W. Kong, and L. Yang, "Drag reduction in cylindrical wake flow using porous material," Phys. Fluids **34**(4), 045102 (2022).
[24]F. Duan and J. Wang, "Fluid–structure–sound interaction in noise reduction of a circular cylinder with flexible splitter plate," J. Fluid Mech. **920**, A6 (2021).
[25]C. Apelt, G. West, and A. A. Szewczyk, "The effects of wake splitter plates on the flow past a circular cylinder in the range $10^4 < Re < 5 \times 10^4$," J. Fluid Mech. **61**(1), 187–198 (1973).
[26]R. Octavianty and M. Asai, "Effects of short splitter plates on vortex shedding and sound generation in flow past two side-by-side square cylinders," Exp. Fluids **57**(9), 143 (2016).
[27]B. Chen, X. Yang, G. Chen, X. Tang, J. Ding, and P. Weng, "Numerical study on the flow and noise control mechanism of wavy cylinder," Phys. Fluids **34**(3), 036108 (2022).
[28]Y. Xing, P. Liu, H. Guo, and L. Li, "Effect of helical cables on cylinder noise control," Appl. Acoust. **122**, 152–155 (2017).
[29]H. Fujita, H. Suzuki, A. Sagawa, and T. Takaishi, "The aeolian tone characteristics of a circular cylinder in high Reynolds number flow," AIAA Paper No. 99-1849, 1999.
[30]A. Lauterbach, K. Ehrenfried, S. Loose, and C. Wagner, "Microphone array wind tunnel measurements of Reynolds number effects in high-speed train aeroacoustics," Int. J. Aeroacoustics **11**(3–4), 411–446 (2012).
[31]W. Terra, A. Sciacchitano, and F. Scarano, "Cyclist Reynolds number effects and drag crisis distribution," J. Wind Eng. Ind. Aerodyn. **200**, 104143 (2020).
[32]K. Zhao, P. Okolo, E. Neri, P. Chen, J. Kennedy, and G. J. Bennett, "Noise reduction technologies for aircraft landing gear: A bibliographic review," Prog. Aerosp. Sci. **112**, 100589 (2020).
[33]T. Zhou, Y. Sun, R. Fattah, X. Zhang, and X. Huang, "An experimental study of trailing edge noise from a pitching airfoil," J. Acoust. Soc. Am. **145**(4), 2009–2021 (2019).
[34]P. Zhou, S. Zhong, and X. Zhang, "On the effect of velvet structures on trailing edge noise: Experimental investigation and theoretical analysis," J. Fluid Mech. **919**, A11 (2021).
[35]R. Amiet, "Refraction of sound by a shear layer," J. Sound Vib. **58**(4), 467–482 (1978).
[36]G. Comte-Bellot, "Hot-wire anemometry," Annu. Rev. Fluid Mech. **8**(1), 209–231 (1976).
[37]O. Phillips, "The intensity of aeolian tones," J. Fluid Mech. **1**(6), 607–624 (1956).
[38]H. Fujita, "The characteristics of the aeolian tone radiated from two-dimensional cylinders," Fluid Dyn. Res. **42**(1), 015002 (2010).
[39]W. Yi, P. Zhou, Y. Fang, J. Guo, S. Zhong, X. Zhang, X. Huang, G. Zhou, and B. Chen, "Design and characterization of a multifunctional low-speed anechoic wind tunnel at HKUST," Aerosp. Sci. Technol. **115**, 106814 (2021).
[40]M. Nishimura, T. Kudo, and M. Nishioka, "Aerodynamic noise reducing techniques by using pile-fabrics," AIAA Paper No. 99-1847, 1999.
[41]S. Singh and S. Mittal, "Flow past a cylinder: Shear layer instability and drag crisis," Int. J. Numer. Methods Fluids **47**(1), 75–98 (2005).
[42]C. Farell and J. Blessmann, "On critical flow around smooth circular cylinders," J. Fluid Mech. **136**, 375–391 (1983).
[43]C. Norberg, "Fluctuating lift on a circular cylinder: Review and new measurements," J. Fluids Struct. **17**(1), 57–96 (2003).
[44]J. S. Cox, K. S. Brentner, and C. L. Rumsey, "Computation of vortex shedding and radiated sound for a circular cylinder: Subcritical to transcritical Reynolds numbers," Theor. Comput. Fluid Dyn. **12**(4), 233–253 (1998).
[45]A. Rinoshika and Y. Zhou, "Orthogonal wavelet multi-resolution analysis of a turbulent cylinder wake," J. Fluid Mech. **524**, 229–248 (2005).
[46]J. S. Humphreys, "On a circular cylinder in a steady wind at transition Reynolds numbers," J. Fluid Mech. **9**(4), 603–612 (1960).
[47]H. Higuchi, H.-J. Kim, and C. Farell, "On flow separation and reattachment around a circular cylinder at critical Reynolds numbers," J. Fluid Mech. **200**, 149–171 (1989).

13 January 2025 06:10:20

Published under an exclusive license by AIP Publishing